12.05

Study of $Y_{3-x}Dy_xFe_5O_{12}$ ($x = 0.0, 0.5, 1.0, 1.5, 3.0$) ferrite garnet for various applications

© A.S. Kamzin[1], J. Xu[2], H. Shen[2,3], V.G. Semenov[4], L.S. Kamzina[1], A.V. Kopylov[5]

[1] Ioffe Institute,
St. Petersburg, Russia
[2] Institute of Crystal Growth, School of Materials Science and Engineering, Shanghai Institute of Technology,
Shanghai, China
[3] State Key Laboratory of Crystal Materials, Shandong University,
Ji'nan, China
[4] St. Petersburg State University,
St. Petersburg, Russia
[5] JSC „Ritvetc",
St. Petersburg, Russia

E-mail: Askam@mail.ioffe.ru

Received October 22, 2025
Revised October 22, 2025
Accepted October 29, 2025

A series of single crystals of the $Y_{3-x}Dy_xFe_5O_{12}$ solid solution ($x = 0.0$, 0.5, 1.0, 1.5, 3.0) synthesized by the Bridgman method was studied. An X-ray diffractometer was used to characterize the properties of the synthesized crystals. The magnetic properties of the crystals were measured using a vibrating-coil magnetometer. Mössbauer studies were conducted using particles obtained by milling the synthesized single crystals. The phase state, the effect of Dy on the crystal properties, and the distribution of iron ions across sublattices were studied using Mössbauer measurements. The obtained results are important for controlling the properties of rare-earth iron garnets for use in optical switches, uncoupled devices, and biomedical applications.

Keywords: magnetic particles, surface properties, Mössbauer spectroscopy.

DOI: 10.61011/PSS.2025.11.62969.289-25

1. Introduction

Rare-earth garnet ferrites $R_3Fe_5O_{12}$ (RIG), where R is a rare-earth element, possess a wide range of magnetic, electric, optical, electromagnetic and magnetooptical properties. All of this makes them promising for use in magnetooptical devices, fiber optic communications, high-power lasers, spintronics, microwave equipment, circulators, phase shifters, in 5G wireless communications [1–5]. RIG particles are promising for biomedical applications, in particular, magnetic resonance imaging, magnetic hyperthermia [6,7]. Such various applications require development of the technologies to obtain the specified characteristics and to research the properties — both of the produced RIG particles and with the substitution with various metals [1,2,6–21]. It was shown that $Y_3Fe_5O_{12}$ particles are highly capable of heat generation in the external alternating magnetic field [16], which is required for magnetic hyperthermic therapy. Particles of yttrium garnet ferrite doped with Sc ions stop being heated by the alternating magnetic field when they reach $\sim 45\,^{\circ}C$, which is important for the magnetic hyperthermia, because at high temperatures the body live cells die [19].

Magnetic properties of RIG are formed due to superexchange interactions of cations of non-equivalent tetrahedral and octahedral positions through the oxygen ions. Therefore, the magnetic characteristics of RIG may be controlled through a change in the distribution of cations among non-equivalent positions, using various synthesis technologies [7,20], and through RIG doping with various ions [1,7,9,10,20,21].

Various methods are used to study the garnet ferrites. The informative ones among them include Mössbauer and Raman-scattering spectroscopy, as highly sensitive to the local environment of the atoms and making it possible to retrieve the detailed information on the complicated structures and exchange interactions, which the iron-containing materials possess [6–16]. High sensitivity of Mössbauer effect to nuclear hyperfine interactions makes it possible to set the parameters of the iron ions in the non-equivalent positions of iron ions in a crystal lattice, which is unavailable for other available methods [22–25].

Ferromagnetic garnets have cubic structure (spatial group Ia3d); each cell contains eight molecules $R_3^{+3}Fe_5^{3+}O_{12}$, and ion distribution may be presented by recording the garnet formula as $\{R_3\}[Fe_2](Fe_3)O_{12}$; where brackets { }, [ ] and ( ) relate to ions in 24c (dodecahedral), 16a (octahedral) and 24d (tetrahedral) sublattices, respectively [26]. Garnet ferrites with ions Fe^{3+}, substituted by a rare-earth element R, are ferrimagnetics, in the crystal lattice of which ions Fe^{3+} occupy two non-equivalent positions 16a and 24d, joined in an antiferromagnetic manner.

Mössbauer studies of RIG are the subject of many papers [6–18,27–33]. In Mössbauer spectra (MS) of RIG there are usually two Zeeman sextuplets (ZS) with wide lines that belong to Fe ions, which occupy the positions in two non-equivalent sublattices in the crystal lattice of the garnet ferrite. In early publications the analysis of MS $Y_3Fe_5O_{12}$ applied the model of two ZS with wide lines that belong to octa- and tetra-sublattices [28–30]; later — with three ZS, one that belongs to ions Fe^{3+} in d-positions, and two others — to ions Fe^{3+} in a1 and a2 positions [27,31]. In [9,10] the MS $Y^3Fe_5O_{12}$ were described with three ZS, for octa-Fe^{3+}, and four ZS for tetra-ions. The quantity and parameters of these ZS are defined by the occupation of positions, the angles between the main axis of the electric field gradient tensor and the light magnetization axis [7,9,10].

This study is dedicated to the analysis of the dependence between the dimensions, cation distribution, crystalline and magnetic structures of the surface layer and the volume of particles and the perfection of the yttrium garnet ferrite crystals when substituted with the Dy ions: $Y_{3-x}Dy_xFe_5O_{12}$ ($x = 0.0, 0.5, 1.0, 1.5, 3.0$).

2. Experimental part

2.1. Synthesis of single crystals, preparation of particles $Y_{3-x}Dy_xFe_5O_{12}$ ($x = 0.0, 0.5, 1.0, 1.5, 3.0$)

Garnet ferrite crystals may be synthesized with various methods [14]: co-precipitation, hydrothermal, sol-gel, pulse laser precipitation etc., The synthesis of high quality macrocrystals of rare-earth garnet ferrites by the Bridgman's method was first proposed in [34]. To synthesize crystals, raw materials Y_2O_3 ($\geq 99.99\,\%$), Dy_2O_3 ($\geq 99.99\,\%$) and Fe_2O_3 ($\geq 9.99\,\%$), weighed in accordance with the stoichiometric ratio, were used, to produce $Y_{3-x}Dy_xFe_5O_{12}$ ($x = 0$, 0.5, 1.0, 1.5, 3.0). The raw materials were thoroughly mixed and baked at 1100 °C for 12 h. The obtained polycrystalline powders $Y_{3-x}Dy_xFe_5O_{12}$ were mixed with flux PbO-B_2O_3 at a mole ratio of $Y_{3-x}Dy_xFe_5O_{12}$: Flux = 30−40 : 70−60. The mixed powders were loaded and sealed in a platinum crucible and moved to the vertical Bridgman's furnace. The furnace was heated to 1200−1250 °C and maintained for 24 h, so that the Dy : YIG powder could fully melt to form a homogeneous solution. Due to high temperature gradient, the high-temperature solution hardened fast, and Dy : YIG crystals were grown with the pulldown rate of 0.2−0.5 mm/h and cooling rate of 0.3−0.5 °C/h. After most of the solution crystallized, the furnace was cooled down to room temperature with the rate of 50−80 °C/h. Single crystals $Y_{3-x}Dy_xFe_5O_{12}$ were extracted from the grown ingot by mechanical removal of flux. The specimens for the Mössbauer measurements were prepared by grinding synthesized single crystals. The produced particles were placed into a special plastic container to eliminate the interaction with the environment.

2.2. Research procedures

Structural analysis and phase identification of the obtained macrocrystals were carried out using X-ray diffractometer (Rigaku MiniFlex 600) with Cu-K emission and wavelength $\lambda = 0.15406$ nm in the stepwise scanning mode (0.02 deg/s) in the range from 20 to 80°. The phase composition of the synthesized crystals was determined by an X-ray diffraction profile using X-ray diffractometer (XRD Shimadzu-6100) with Cu-Kα emission and wavelength 0.15420 nm.

Due to high sensitivity of Mössbauer effect to the nuclear hyperfine interactions it is possible to make an unambiguous identification of iron oxides, which have very close values of the crystal lattice constants, which is unavailable in other procedures [23–26]. Besides, this method easily identifies Fe^{2+} and Fe^{3+} ions. For Mössbauer studies of the magnetic structure and phase state of the sample structure perfection degree, distribution of Fe^{3+} ions in the crystal lattice in non-equivalent octa- (a) and tetra-positions (d), a Mössbauer spectrometer was used in the synthesized garnet ferrites with registration of γ-quanta from a Co^{57}(Rh) source in the geometry of transmittance through the sample. Motion of γ-quanta ^{57}Co(Rh) source with an activity of 50 mCi in a Doppler modulator of the spectrometer was controlled via a triangular reference signal to specify a constant-acceleration speed. The rate scale was calibrated using α-Fe foil with thickness of 6 μm at room temperature. The Mössbauer effect was measured on the particles produced by grinding the synthesized single crystals $Y_{3-x}Dy_xFe_5O_{12}$. $Y_{3-x}Dy_xFe_5O_{12}$ particles were placed into plastic containers to prevent interaction with the ambient air. The experimental MS mathematical processing was carried out using the specialized software [35], which describes spectral lines with Lorentzian peaks using the least-square method. The divergence of theoretical values of the hyperfine interaction (HFI) parameters is determined from the statistical deviations. The software procedure of functional minimization $\chi 2$ includes searching for optimal values of the such parameters of spectral lines as widths, intensities and positions. Positions of the spectral lines are used to calculate HFI parameters: IS — the isomer shift, QS — the quadrupolar splitting, H_{eff} — the effective magnetic field.

3. Results and discussion

3.1. X-ray diffraction analysis of crystals $Y_{3-x}Dy_xFe_5O_{12}$

Experimental X-ray diffraction patterns (XRD) of $Y_{3-x}Dy_xFe_5O_{12}$ garnets are shown in Figure 1. It should be noted that XRDs are similar to the ones published for $Dy_3Fe_5O_{12}$ [33,36], $Y_3Fe_5O_{12}$ [7,9,10–12,28,33] and $Y_{3-x}Dy_xFe_5O_{12}$ [9,10,17,36]. Diffraction peaks indicated in Figure 1, correspond to the planes (220), (311), (400), (511) and (440), indicate that the structure of the studied particles $Y_3Fe_5O_{12}$ corresponds to the cubic structure

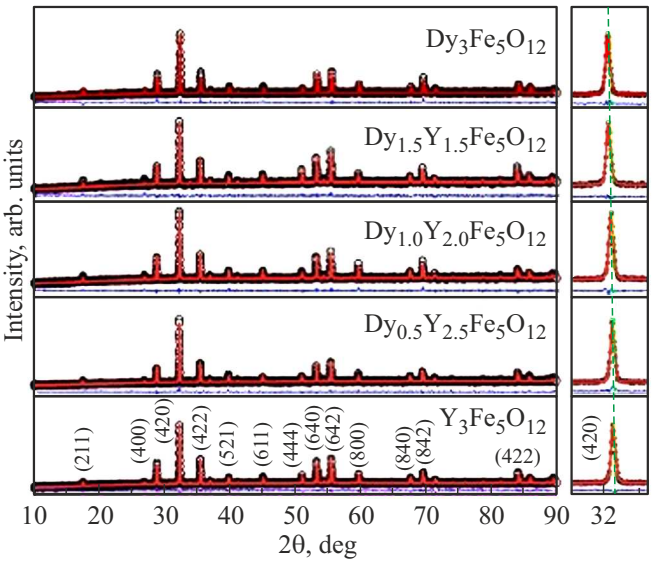

Figure 1. X-ray diffraction patterns of $Y_{3-x}Dy_xFe_5O_{12}$ ($x = 0$, 0.5, 1.0, 1.5, 3) crystals and line shift (420).

Table 1. Confirmed structural parameters of crystals $Y_{3-x}Dy_xFe_5O_{12}$

x	Parameter of lattice, nm	Bond angle, deg Fe1−O−Fe$_2$	Bond length, nm	
			Fe1−O	Fe2−O
0.0	1.2379	128.48	0.1983	0.1858
0.5	1.2391	128.50	0.1985	0.1860
1.0	1.2395	128.56	0.1986	0.1861
1.5	1.2401	128.91	0.1987	0.1862
3.0	1.2420	129.67	0.2027	0.1861

(JCPDS No. 73-1377), and for the ones doped with ions Dy ($Y_{3-x}Dy_xFe_5O_{12}$) — to the parameters of JCPDS cards No. 73-1964, JCPDS No. 10-0319 and No. 74-2403.

The position of the most intense diffraction peak (420), as the content of ions Dy^{3+} increases, moves towards smaller angles, which indicates the increased size of the crystal lattice. The confirmed parameters of the lattice cell are presented in Table 1.

As the content of Dy3+ ions increases, the size of the lattice increases from 1.2379 to 1.2420 nm, which agrees with the data of papers [32,36,37]. Saturation magnetization M_s, for $Y_3Fe_5O_{12}$ being 23.62 emu/g, decreases down to 5.33 emu/g when Dy is introduced. The coercivity field remains unchanged at the same time.

3.2. Experimental Mössbauer spectra of room temperature for particles $Y_{3-x}Dy_xFe_5O_{12}$

The reason of using powders of ground single crystals for Mössbauer measurements consists in the fact that the synthesis of single-phase RIG particles greatly depends on some chemical factors and temperature of synthesis [7], and the properties of macroscopic crystals may vary significantly from the properties of synthesized particles of the same composition.

3.3. Analysis of Mössbauer spectra $Y_{3-x}Dy_xFe_5O_{12}$

The Mössbauer spectra of $Y_{3-x}Dy_xFe_5O_{12}$ particles, where $x = 0.0$, 0.5, 1.0, 1.5, 3.0, obtained at 295 K, are shown in Figure 2. In MS (Figure 2) one can see two ZS with rather good resolution of lines, which is similar to RIG MS. Mathematical processing of experimental MS (Figure 2) was conducted using „MOSFIT“ [35] software with a model consisting of four ZS. Such processing of MS (Figure 2) led to rather satisfactory results for value χ^2, which was within 0.25 to 1.1. The value χ^2 is a criterion of the used models compliance with the experimental spectra. The criterion of such compliance is also the difference of

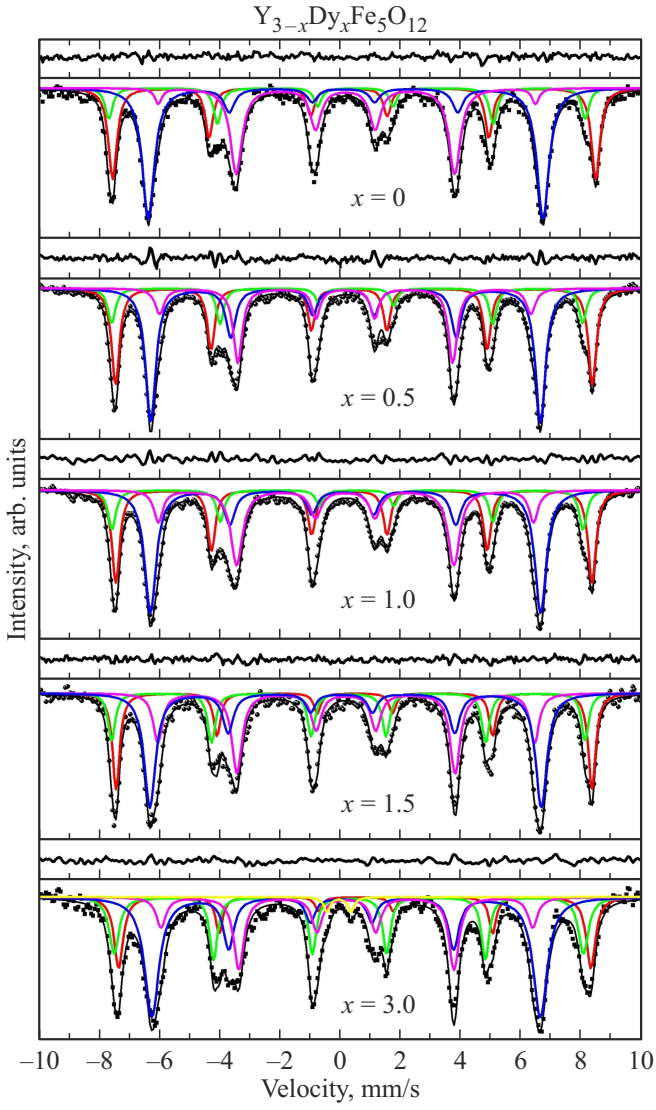

Figure 2. Mössbauer spectra of particles $Y_{3-x}Dy_xFe_5O_{12}$ ($x = 0.0$, 0.5, 1.0, 1.5, 3.0).

the model presentations and experimental spectra shown in Figure 2 above every spectrum. These differences are minimum, which indicates a proper match of the used models and the experimental data, and same as value χ^2, it indicates the reliability of such processing. The experimental values of MS are shown by dots (Figure 2), whereas the model components obtained by mathematical analysis of MS using software [35] are shown by color lines.

The selection of the models describing MS (Figure 2) was carried out on the basis of the fact that garnet ferrimagnetism was formed by two non-equivalent magnetic sublattices, namely from iron atoms in (16) octa- and in (24) tetrahedral positions joined in an antiferromagnetic manner. Therefore, MS of single-crystal garnet ferrite consists of the components corresponding to several octa- and tetrahedral structural positions Fe^{3+} in the oxygen environment [37], the quantity and parameters of which are determined by the occupancy of the positions, angles θ between the main axis of the electric field gradient tensor main axis and the axis of light magnetization. The synthesis resulted in the formation of the garnet phase with certain distortions of the crystalline and magnetic structures. Orientation of the main axis of the electric field gradient tensor relative to direction [111] varies because of distortions [7,28]. Therefore, to describe the octahedral Fe^{3+} ions, two ZS were used with the characteristics given in Table 2. As for ZS iron ions in tetra-positions, the large width of the lines of this ZS allows simulation with two, three (or more) ZS. We attempted to describe Fe tetra- ions on MS (Figure 2) with three or four ZS, similarly used in [7,9,10], but the result was negative. As a result, ZS of Fe^{3+} ions in tetra-positions were described by two ZS (Figure 2); model for MS $Y_{3-x}Dy_xFe_5O_{12}$ consists of four ZS that belong to ions Fe^{3+}, and in case of particles $Dy_3Fe_5O_{12}$ a doublet was added.

The HFI parameters were calculated using the positions of spectral lines in MS of particles $Y_{3-x}Dy_xFe_5O_{12}$: isomeric shifts (IS), quadrupole splits (QS), effective fields (H_{eff}), presented in Table 2.

It should be noted that in papers [7,12] in process of MS processing the limitations were imposed on the ratios of sextuplets areas, their isomer shifts and quadrupole splits. Free were only the values H_{eff} and angles of orientation of the gradient of the electric and effective field (H_{eff}) [9,10], while in process of processing of experimental MS presented in Figure 2, using MOSFIT software [35] all variable parameters were free.

Mössbauer spectroscopy makes it possible to unambiguously identify Fe^{3+} and Fe_{2+} ions using their chemical shifts making $\sim 0.2-0.5$ and $\sim 0.9-1.1$ mm/s accordingly [24]. Table 2 demonstrates that IS values are within the range of $0.1-0.48$ mm/s, indicating that in the studied particles only ion ions are present in the high-spin state Fe^{3+}.

Impurity phases of iron oxides manifest themselves on MS as additional ZS or doublets with HFI parameters that differ substantially from parameters of the studied compounds. The detection limit of the secondary phase is about 3 at.% of the iron and any impurity phase even with such an iron quantity can be easily determined from MS. Analysis of experimental MS of the studied particles $Y_{3-x}Dy_xFe_5O_{12}$ (Figure 2) did not show the presence of additional lines; therefore, the impurity phases are absent, which confirms the results of Raman and X-ray studies.

Figure 3 presents the dependences of ZS lines of iron ions in the studfied garnet ferrites $Y_{3-x}Dy_xFe_5O_{12}$. In Figure 3 you can see that in the studied garnet ferrites as the number of Dy ions increase, the intensities of the lines of both octa- and tetra-sublattcies change in opposite directions. Therefore, as the number of Dy^{2+} ions increases, the distribution of iron ions changes within the sublattices, which may impact the chemical environment Fe^{3+} in the non-equivalent positions. However, the ratio of the number of iron ions of octa- and tetra-sublattices with the introduction of Dy ions will not change.

The width values of the lines (Table 2) show that the signs of high disorder in a B-sublattice are observed for all samples, which is indicated by large width of the spectral lines of this sublattice. Doping with Dy ions practically does not result in the reduction of the effective field for both positions of iron ions. When the number of the introduced Dy ions changes, isomer shifts will not change substantially. This is an additional proof of Fe ion valence stability upon introduction of Dy ions.

Decrease in crystal size to nanovalues causes a change in the properties of the particle surface and appearance of size effects that substantially impact the magnetic properties of the MNPs. For the first time the assumption of a surface layer existence with a different structure in MNPs was made as a result of nanoparticle magnetization studies [37]. It is related to the fact that as the surface/volume ratio increases, as it occurs in MNPs, the surface role increases greatly in the formation of the particle properties. Formation of the anisotropic surface layer, for the first time theoretically predicted by Néel [38] occurs as a result of loss of some superexchange interactions of Fe ions due to such a defect as the surface. Based on the data of Mössbauer studies in strong external fields (SEF), an assumption was made that such a layer existed in the particles of yttrium garnet ferrite [39] and yttrium gadolinium garnet ferrite [40]. However, it should be noted that the proof of existence of the anisotropic layer (surface layer with canted spin structure — CSS) with Mössbauer measurements in strong SEFs are subjected to discussions.

Simulation of MS of the particles of yttrium garnet ferrite demonstrated the presence of ZS with large widths of lines and considerably smaller effective fields [7,12], and the assumption was made that these ZS are related to the iron ions located in the surface layer of the yttrium garnet particles. However, the arguments were not provided for the assumption of formation of such ZS [7,12].

The first direct proof of CSS layer existence on the surface of Fe_3BO_6, $BaM(BaFe_{12}O_{19})$, and also $MAFe_{12}O_{19}$, (where M = Ba or Sr, A = Sc or Al) macrocrystals were presented in [41–47]. These results without the use of

Table 2. The width values of the pairs of the first and sixth (G1) lines of Zeeman sextuplets, isomer shifts (IS), quadrupole splits (QS), effective magnetic fields (H_{eff}) and areas of components (S) for Fe ions in tetraheric (A) and octahedral (B) positions in the particles $Y_{3-x}Dy_xFe_5O_{12}$, at $T = 300$ K

Sample	Position	G1, mm/s	IS, mm/s	QS, mm/s	H_{eff}, T	S, %
$Y_3Fe_5O_{12}$	12k	0.301 ± 0.020	0.385 ± 0.005	0.148 ± 0.010	49.34 ± 0.03	29
	$4f_1$	0.339 ± 0.060	0.388 ± 0.016	0.380 ± 0.033	48.68 ± 0.09	9
	$4f_2$	0.399 ± 0.018	0.107 ± 0.055	0.120 ± 0.108	40.21 ± 0.06	30
	2a	0.232 ± 0.170	0.180 ± 0.019	0.038 ± 0.037	39.03 ± 0.19	32
$Y_{2.5}Dy_{0.5}Fe_5O_{12}$	12k	0.319 ± 0.007	0.374 ± 0.002	0.158 ± 0.004	49.15 ± 0.01	27
	$4f_1$	0.302 ± 0.000	0.384 ± 0.004	0.308 ± 0.008	48.55 ± 0.03	12
	$4f_2$	0.404 ± 0.000	0.143 ± 0.002	0.066 ± 0.004	40.17 ± 0.01	32
	2a	0.369 ± 0.000	0.165 ± 0.004	0.003 ± 0.007	38.26 ± 0.03	29
$Y_{2.0}Dy_{1.0}Fe_5O_{12}$	12k	0.315 ± 0.011	0.377 ± 0.003	0.149 ± 0.006	49.08 ± 0.02	25
	$4f_1$	0.305 ± 0.026	0.392 ± 0.006	0.305 ± 0.012	48.54 ± 0.04	13
	$4f_2$	0.456 ± 0.012	0.128 ± 0.006	0.091 ± 0.012	40.22 ± 0.04	34
	2a	0.358 ± 0.040	0.177 ± 0.005	0.021 ± 0.009	38.67 ± 0.08	28
$Y_{1.5}Dy_{1.5}Fe_5O_{12}$	12k	0.290 ± 0.022	0.470 ± 0.008	0.028 ± 0.016	49.05 ± 0.03	20
	$4f_1$	0.286 ± 0.045	0.273 ± 0.010	0.008 ± 0.021	48.80 ± 0.05	18
	$4f_2$	0.453 ± 0.024	0.108 ± 0.011	0.136 ± 0.020	40.34 ± 0.07	34
	2a	0.369 ± 0.046	0.194 ± 0.006	0.004 ± 0.012	38.83 ± 0.09	28
$Dy_3Fe_5O_{12}$	12k	0.359 ± 0.061	0.504 ± 0.019	0.045 ± 0.038	48.65 ± 0.08	16
	$4f_1$	0.386 ± 0.083	0.296 ± 0.021	0.030 ± 0.041	48.36 ± 0.09	22
	$4f_2$	0.575 ± 0.045	0.106 ± 0.014	0.173 ± 0.026	40.01 ± 0.12	42
	2a	0.384 ± 0.136	0.215 ± 0.017	0.011 ± 0.032	38.33 ± 0.16	18
	D	0.247 ± 0.121	0.033 ± 0.043	0.794 ± 0.085	–	2

HFI parameters given in Table 2 agree with values for Y- [8] and Dy-garnets [9].

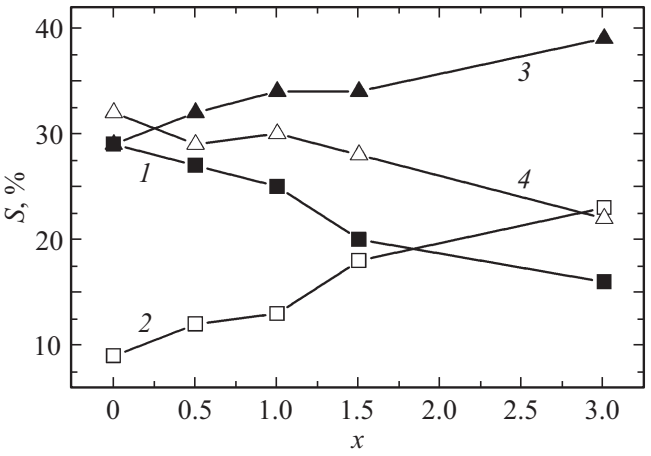

Figure 3. Dependences of ZS lines intensities in MS in the studied garnet ferrites $Y_{3-x}Dy_xFe_5O_{12}$ for $x = 0.0$, 0.5, 1.0, 1.5, 3.0). The curve *1* relates to the sublattice 12k; *2* — to 4f1; *3* — to 4f2; *4* — to 2a.

strong SEFs were obtained using a new unique method of „Simultaneous gamma, X-ray and electronic Mössbauer spectroscopy (SGXEMS)“, proposed in [48–50]. The uniqueness of SGXEMS method consists in the fact that it makes it possible to simultaneously retrieve information on the properties of a thin surface layer and the volume of macroscopic crystals, besides, using only Mössbauer spectroscopy with the simultaneous recording of various emissions, making it possible to directly compare data on the surface layer and volume of crystals. Later the SGXEMS method in foreign literature was called „Simultaneous Triple Radiation Mössbauer Spectroscopy (STRMS)“ [51–52].

For the first time, using the MS analysis of the MNP of nucleus/shell type taken in the geometry of transmission of gamma radiation through the sample without use of high SEFs, data was received, which made it possible to assume that there is a layer with CSS on the surface of the studied particles [23]. MS analysis of spinel ferrites [24–26] also

demonstrated that on the surface of MNP there is a layer with CSS, and the substantiation for such conclusion was provided. Garnet ferrites are the compounds with a cubic structure characterized by high symmetry. Therefore the QS values as you can see in Table 2 are close to zero or are low. Then as in case of $Dy_3Fe_5O_{12}$, as you can see in Figure 2 and in Table 2, there is a doublet present, the quadrupole splitting QS value of which is much higher. The reason for such increase of QS may be the fact that the surface in the particles is a „defect", which substantially damages the cubic structure of the surface layer. As a result, a surface layer is formed, the parameters of which differ from the ones observed in the „volume" of the particle. However, in case of $Dy_3Fe_5O_{12}$ particles, the presence of the doublet with high QS value indicates the existence of a thin surface layer with the properties differing from the volume of the particles,as a result of the damage of the garnet ferrite particle cubic crystalline structure with the surface. The observed quadrupole splitting without ZS in this component in $Dy_3Fe_5O_{12}$ MS indicated the absence of magnetic order, which makes it possible to call this surface layer „magnetically dead" [53]. It should be noted that the layer with CSS observed on the surface of macrocrystals, as it was proven in [41–47], may remain upon grinding, too,

In [18] the observed reduction of saturation magnetization with the reduction in the particle size was explained by the damage of exchange interaction by the surface and formation of a non-magnetic surface layer surrounding the MNP. The magnetic diameter was defined by adapting the magnetization data with Langevin function, and it was shown that the ratio of thickness of „magnetically dead" surface layer to the particle size decreases logarithmically with increase in MNP size [18].

Mathematical processing of MS, as you can see in Figure 2, did not show ZS lines that belong to the layer with CSS on the surface of the studied particles of garnet ferrites similar to the ones observed in [7,12]. Such difference from the results obtained in [7,12], is explained by the fact that [7,12] studied the particles of garnet ferrites of smaller dimensions, where as MS presented in Figure 2 were obtained using large particles. In case of large particles the ratio of the surface/volume decreases greatly, which causes a higher signal from the particle volume, against the background of which the signal from the surface layer is not observed due to its smallness.

4. Conclusion

Mössbauer studies of particles prepared by grinding of $Y_{3-x}Dy_xFe_5O_{12}$ ($x = 0.0, 0.5, 1.0, 1.5, 3.0$) macrocrystals synthesized with Bridgman's method were completed, which made it possible to obtain information on the properties of both single crystals and particles. It is not available when the particles are used that are synthesized by a similar method of synthesis of macrocrystals with the same composition. Features and evolution of the crystalline and magnetic structure were studied by methods of X-ray diffraction, Mössbauer spectroscopy and magnetometry. Mössbauer studies demonstrated that the obtained macrocrystals were garnet ferrites $Y_{3-x}Dy_xFe_5O_{12}$ ($x = 0.0, 0.5, 1.0, 1.5, 3.0$), and no presence of any impurities was found, which confirms the results of Raman and X-ray studies. The experimental Mössbauer spectra were simulated using four Zeeman sextuplets. Analysis of HFI parameters calculated using the results of MS processing demonstrated that two of four ZS belong to Fe ions that occupy tetrahedral FeO_4, and two other ones — octahedral positions of FeO_6 in the crystalline structure of the garnet ferrite. Iron ions in crystals are in high-spin state Fe^{3+}, iron ions in low-spin state Fe^{2+} are unavailable.

As the number of the substituting Dy ions increases, the intensities of the lines of both octa- and tetra-sublattices vary in the opposite directions. Therefore, as the number of Dy^{2+} ions increases, the distribution of iron ions changes within the sublattices, which may impact the chemical environment Fe^{3+} in the non-equivalent positions. The ratio of the intensities of the lines that belong to octa- and tetra-sublattices remains constant and does not depend on the number of the introduced Dy ions. This means that as the content of Dy increases in the crystals, the total population of octa- and tetra-positions does not change, but the ion distribution in the sublattices as such changes. Doping with Dy ions does not result in the reduction of the effective field for both positions of iron ions. However, when the number of the introduced Dy ions changes, isomer shifts will not change substantially. This is an additional proof of Fe ion valence stability upon introduction of Dy.

The model interpretation of Mössbauer spectra (Figure 2) did not find the presence of surface and volume components caused by the surface effect as it is observed with the nanoscale particles. This is explained by the fact that the studies used particles of garnet ferrites with size of more than 150 nm. However, in case of $Dy_3Fe_5O_{12}$ particles, the presence of the doublet with high QS value indicates the existence of a thin surface layer with the properties differing from the volume of the particles. Absence of the magnetic order in this layer indicates that this layer is „magnet-dead".

Conflict of interest

The authors declare that they have no conflict of interest.

References

[1] H. Shen, Y. Zhao, L. Li, Q. Li, H. Geng, Y. Li, X. Shen, J. Xu, D. Zhou, T. Tian, Y. Ma, J. Shang, A. Wu. J. Cryst. Growth **631**, 127626 (2024). https://doi.org/10.1016/j.jcrysgro.2024.127626

[2] L. Zhang, D. Hu, I.L. Snetkov, S. Balabanov, O. Palashov, J. Li. J. Adv. Ceram. **12**, *5*, 873 (2023). https://doi.org/10.26599/JAC.2023.9220742

[3] K.J. Carothers, R.A. Norwood, J. Pyun. Chem. Mater. **34**, *6*, 2531 (2022). https://doi.org/10.1021/acs.chemmater.2c00158

[4] J. Qin, S. Xia, W. Yang, H. Wang, W. Yan, Y. Yang, Z. Wei, W. Liu, Y. Luo, L. Deng, L. Bi. Nanophotonics **11**, *11*, 2639 (2022). https://doi. org/10.1515/nanoph-2021-0719
[5] K. Srinivasan, B.J.H. Stadler. Opt. Mater. Express. **12**, *2*, 697 (2022). https://doi.org/10.1364/OME.447398
[6] R. Fopase, V. Saxena, P. Seal, J.P. Borah, L. M. Pandey. Mater. Sci. Eng. C **116**, 111163 (2020).
[7] T. Kiseleva, R. Abbas, K. Martinson, A. Komlev, E. Lazareva, P. Tyapkin, E. Solodov, V. Rusakov, A. Pyatakov, A. Tishin, N. Perov, E. Uyanga, D. Sangaa, V. Popkov. Nanomater. **12**, *16*, 2733 (2022). https://doi.org/10.3390/nano12162733
[8] V.G. Kostishin, V.V. Korovushkin, A.G. Nalogin, S.V. Shcherbakov, I.M. Isaev, A.A. Alekseev, A.Yu. Mironovich, D.V. Salogub. Phys. Solid State **62**, *7*, 1156 (2020).
[9] D. Vandormael, F. Grandjean, D. Hautot, G.J. Long. J. Phys. Condens. Matter. **13**, *8*, 1759 (2001).
[10] G.J. Long, F. Grandjean, X. Guo, A. avrotsky, R.K. Kukkadapu. Inorg. Chem. **55**, *7*, 3413 (2016). https://doi.org/10.1021/acs.inorgchem.5b02769
[11] R. Abbas, K.D. Martinson, T.Y. Kiseleva, G.P. Markov, P.Y. Tyapkin, V.I. Popkov. Mater. Today Commun. **32**, 103866 (2022). https://doi.org/10.1016/j.mtcomm.2022.103866
[12] T.Yu. Kiseleva, V.S. Rusakov, R. Abbas, E.V. Lazareva, P.Yu. Tyapkin, K.D. Martinson, A.S. Komlev, N.S. Perov, V.I. Popkov. Crystallogr. Rep. **68**, *3*, 478 (2023). https://doi.org/10.1134/S1063774523700190
[13] D. Neupane, N. Kramer, R. Bhattarai, C. Hanley, A.K. Pathak, X. Shen, S. Karna, S.R. Mishra. Ceram. **6**, *4*, 1937 (2023). https://doi.org/10.3390/ceramics6040120
[14] H. Aono, H. Ebara, R. Senba, T. Naohara, T. Maehara, H. Hirazawa, Y. Watanabe. J. Am. Ceram. Soc. **94**, *12*, 4116 (2011). https://doi.org/10.1111/j.1551-2916.2011.04879.x
[15] W. Zhou, J. Ye, S. Zhuo, D. Yu, P. Fang, R. Peng, Y. Liu, W. Chen. J. Alloys Compd. **896**, 162883 (2022). https://doi.org/10.1016/j.jallcom.2021.162883
[16] H. Hirazawa, R. Matsumoto, M. Sakamoto, U. Enkhnaran, D. Sangaa, T.Yu. Kiseleva, J. Yano, H. Fukuoka, H. Aono. J. Ceram. Soc. Jpn. **129**, *9*, 579 (2021). http://doi.org/10.2109/jcersj2.21058
[17] M. Lataifeh, Q.I. Mohaidat, S.H. Mahmood, I. Bsoul, M. Awawdeh, I. Abu-Aljarayesh, M. Altheeba. Chin. Phys. B **27**, *10*, 107501 (2018). https://doi.org/10.1088/1674-1056/27/10/107501
[18] M. Niyaifar, H. Mohammadpour, M. Dorafshani, A. Hasanpour. J. Magn. Magn. Mater. **409**, 104 (2016). http://dx.doi.org/10.1016/j.jmmm.2016.02.097
[19] A.T. Apostolov, I.N. Apostolova, J.M. Wesselinowa. Physica Status Solidi B **259**, *3*, 2100545 (2022). https://doi.org/10.1002/pssb.202100545
[20] M.N. Akhtar, M.A. Khan, M. Ahmad, G. Murtaza, R. Raza, S.F. Shaukat, M.H. Asif, N. Nasir, G. Abbas, M.S. Nazir, M.R. Raza. J. Magn. Magn. Mater. **368**, 393 (2014). http://doi.org/10.1016/j.jmmm.2014.06.004
[21] K. Sadhana, S.R. Murthy, K. Praveena. Mater. Sci. Semicond. Process. **34**, 305 (2015). http://doi.org/10.1016/j.mssp.2015.02.056
[22] V. Kuncser, O. Crisan, G. Schinteie, F. Tolea, P. Palade, M. Valeanu, G. Filoti. Modern Trends in Nanoscience, v. 197. Editura Academiei Romane, Bucharest (2013).
[23] A.S. Kamzin, I.M. Obaidat, A.A. Valliulin, V.G. Semenov, I.A. Al-Omari. Phys. Solid State **62**, *10*, 1933 (2020). https://doi.org/10.1134/S1063783420100157.
[24] A.S. Kamzin, G. Caliskan, N. Dogan, A. Bingolbali, V.G. Semenov, I.V. Buryanenko. Phys. Solid State **64**, *10*, 1550 (2022). https://doi.org/10.21883/PSS.2022.10.54249.391
[25] A.S. Kamzin, I.M. Obaidat, V.G. Semenov, V. Narayanaswamy, I.A. Al-Omari, B. Issa, I.V. Buryanenko. Phys. Solid State **65**, *3*, 470 (2023). https://doi.org/10.21883/PSS.2023.03.55591.544
[26] A.S. Kamzin, V.G. Semenov, L.S. Kamzina. Phys. Solid State **66**, *4*, 603 (2024). DOI: 10.61011/PSS.2024.04.58207.44
[27] S. Geller. Z. Kristallogr. **125**, *1*(1967). Z. Kristallogr. **125**, *1–6*, 1 (1967).
[28] G.A. Sawatzky, F. Van der Woude, A.H. Morrish. Phys. Rev. **183**, *2*, 383 (1969). https://doi.org/10.1103/PhysRev.183.383
[29] V.K. Sankaranarayanan, N.S. Gajbhiye. J. Mater. Sci. **29**, *3*, 762 (1994).
[30] M.S. Lataifeh, A.-F.D. Lehlooh. Solid State Commun. **97**, *9*, 805 (1996).
[31] J.M. Greneche, H. Pascard, J.R. Regnard. Solid State Commun. **65**, *7*, 713 (1988).
[32] H. Winkler, R. Eisberg, E. Alp, R. Rüffer, E. Gerdau, S. Lauer, A.X. Trautwein, M. Grodzicki, A. Vera. Z. Physik B Condens. Matter **49**, *4*, 331 (1983).
[33] M. Guillot, C.N. Chinnasamy, J.M. Greneche, V.G. Harris. J. Appl. Phys. **111**, *7*, 07A517 (2012). https://doi.org/10.1063/1.3679020
[34] Y. Jiang, H. Shen, J. Xu, J. Ma, H. Wang, B. Lu. J. Rare Earths **39**, *12*, 1547 (2021). https://doi.org/10.1016/j.jre.2021.03.020
[35] V.G. Semenov, V.V. Panchuk. Programma obrabotki messbauerovskikh spectrov MossFit. Chastnoe soobshchenie (in Russian)
[36] A.B. Bhosale, S.B. Somvanshi, V.D. Murumkar, K.M. Jadhav. Ceram. Int. **46**, *10* Part A, 15372 (2020). https://doi.org/10.1016/j.ceramint.2020.03.081
[37] A.E. Berkowitz, W.J. Schuele, P.J. Flanders. J. Appl. Phys. **39**, *2*, 1261 (1968).
[38] L. Neel. J. Physique. Radium **15**, *4*, 225 (1954).
[39] K. Haneda, A.H. Morrish. J. Magn. Soc. Jpn. **22**, *S_1_ISFA_*97, 255 (1998). https://doi.org/10.3379/jmsjmag.22.S1_255
[40] M. Kuila, M.K. Mardegan, A. Tayal, C. Meneghini, S. Francoual, V.R. Reddy. J. Phys.: Cond. Matter **35**, *44*, 445801 (2023). https://doi.org/10.1088/1361-648X/acea11
[41] A.S. Kamzin, L.A. Grigor'ev. JETP Lett. **57**, *9*, 557 (1993).
[42] A.S. Kamzin, L.A. Grigor'ev. JETP **77**, *4*, 658 (1993).
[43] A.S. Kamzin, L.P. Ol'khovik, V.L. Rozenbaum. JETP Lett. **61**, *11*, 936 (1995).
[44] A.S. Kamzin. JETP **89**, *5*, 891 (1999).
[45] A.S. Kamzin, L.P. Ol'khovik, V.L. Rozenbaum. Phys. Solid State **41**, *3*, 433 (1999).
[46] A.S. Kamzin, V.L. Rozenbaum, L.P. Ol'khovik. JETP Lett. **67**, *10*, 843 (1998).
[47] A.S. Kamzin, L.P. Ol'khovik. Phys. Solid State **41**, *10*, 1658 (1999).
[48] A.S. Kamzin, V.P. Rusakov, L.A. Grigoriev. Physics of Transition Metals. Int. Conf. USSR (1988). Proc. Pt. II. P. 271.
[49] A.S. Kamzin, L.A. Grigoriev. Pisma v ZhTF **16**, *16* 38 (1990). (in Russian).
[50] A.S. Kamzin, L.A. Grigoriev. ZhTF **60**, *7*, 151 (1990). (in Russian).
[51] F. Schaaf, U. Gonser. Hyperfine Interact. **57**, *1*, 2101 (1990).
[52] U. Gonser, P. Schaaf, F. Aubertin. Hyperfine Interact. **66**, *1*, 95 (1991).
[53] E. Umut, M. Coşkun, H. Güngüneş, V. Dupuis, A.S. Kamzin. J. Supercond. Novel Magn. **34**, *3*, 913 (2021). https://doi.org/10.1007/s10948-020-05800-y

Translated by M.Verenikina